Check for updates

RESEARCH ARTICLE

CRYSTAL Research&Technology

www.crt-journal.org

Production and Characterization of Electrodeposited Cadmium Sulfide Semiconductor Films with Different Boron Content

Erman Erdoğan

In this study, Cadmium Sulfide (CdS) semiconductor films are electrodeposited on Indium Tin Oxide (ITO) substrates at 80 °C base temperature for different boric acid (H_3BO_3) ratios. The effect of boric acid on these films is investigated. For this, first of all, the structural change of the films is examined. Among the films obtained with different boric acid ratios, the optimum film is achieved with 0.06 M boric acid doped. From the basic absorption spectra ($\alpha h\upsilon$) of the obtained CdS:B films, the variation of $h\upsilon$ is drawn and it is determined that the CdS:B semiconductor films has a direct band transition. From the basic absorption spectra of the obtained CdS:B films, it is observed that the CdS:B semiconductor films has a direct band transition. In addition, the optical energy bandgap values obtained are in agreement with the values in the available literatures. The results of the structural, optical, and morphological properties of the films produced in this study indicate that among the selected additive ratios, 1% boric acid gives the best and optimum deposition condition. The thin films obtained are also found to be useful as absorber layers in photovoltaic solar cells.

1. Introduction

Semiconductor materials are widely used in technology because their electrical and optical properties can be altered. Thin films are the most preferred materials due to the use of less material and the change in the properties of nano-sized materials. Thin films are used as materials in advanced technologies due to their attractive chemical, optical, magnetic, and mechanical properties.[1] CdS is an II–VI group compound consisting of the combination of cadmium (Cd) from group II elements and sulfur (S) from group VI elements of the periodic table.[2] Binary compounds of group II-VI are of great importance due to their applications in various optical and electronic devices. Semiconductor CdS compound has a wide range of uses considering its desirable electrical and optical properties, especially in devices such as solar cells, photodetectors, and field-effect transistors.[3] CdS, can be in either cubic or hexagonal structure, or it is one of the compounds that can contain both types in its structure.[4] CdS thin films have a wide range of applications in solid-state lasers, detectors, solar cells, and photovoltaic applications.[5] Since their bandgaps are ≈2.42–2.58 eV, they have the property of emitting light in the green spectral region.[6] CdS films are used as window materials in heterojunction solar cells because of their wide bandgap, high transmittance, and low-cost techniques. Research indicated that CdS thin films have been produced by different deposition techniques, such as; evaporation,[7] RF sputtering,[8] spray pyrolysis,[9] chemical bath,[10] pulsed laser deposition [11] and electrodeposition.[12] Within these deposition techniques, electrodeposition is considered one of the low-cost methods for semiconductor thin film fabrication. Electrodeposition is the deposition of ionic materials as a thin layer on the surface of a conductive substrate in a solution of ionic type material.[13]

H_3BO_3 is the product of the hydrolysis of boron compounds and is usually produced by acidifying an aqueous solution of borax. It is used in the glass and ceramics industry, agriculture, nuclear applications, boron alloys, the textile industry, and many more applications.[14] The applications of boron to CdS thin films, which are used as optical windows in solar cells resistant to ultraviolet rays are not seen much in the literature. However, it is known that boron is an element that can enter Cd spaces or intermediate places within the CdS structure and increases the resistance of the structure to radiation. B^{+3}(2.04) has higher electronegativity than Cd^{+2}(1.86) and the ionic radius of B^{+3}(41 pm) is smaller than the ionic radius of Cd^{+2}(109 pm). Since the boron element has an empty p orbital, it generally behaves as a Lewis acid, in other words, it easily bonds with electron-rich compounds and eliminates the need for electrons.[15]

In this study, boron-doped CdS samples were deposited by electrodeposition technique, followed by doping at different boron concentrations in mixed cadmium chloride ($CdCl_2$) and sodium thiosulfate ($Na_2S_2O_3$) initial solutions. The effects of doping on optical, structural, and surface morphologies were investigated.

E. Erdoğan
Electronic Communication Technology Program, Vocational High School
Bilecik Seyh Edebali University
Bilecik 11100, Turkey
E-mail: erman.erdogan@bilecik.edu.tr

The ORCID identification number(s) for the author(s) of this article can be found under https://doi.org/10.1002/crat.202300353

DOI: 10.1002/crat.202300353

 © 2024 Wiley-VCH GmbH

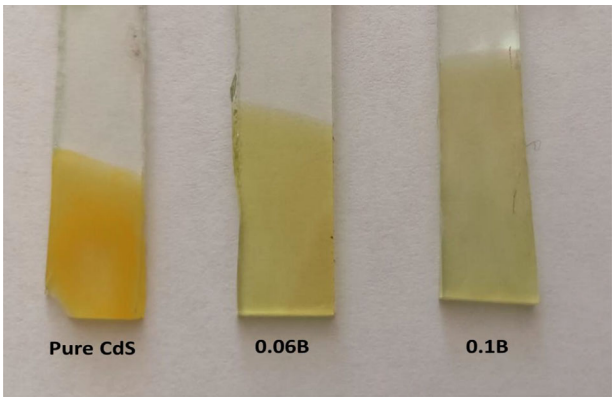

Figure 1. Pictures of the pure and boron-doped CdS thin films.

2. Experimental Section

The chemicals used during the experiment were $Na_2S_2O_3$ as a source of sulfur, H_3BO_3 as a boron source, and $CdCl_2$ as a source of cadmium. First, ITO-coated thin glass films were cut in 1 × 2 cm dimensions, washed with distilled water, and kept in an ultrasonic vibrator for 10 min. The films were bathed in acetone, isopropanol, and distilled water successively for 10 min each. After cleaning, it was quickly dried using nitrogen gas. The pH value of the solution prepared in a separate container was adjusted to 2.5 using hydrochloric acid. The solutions used in the experiment were prepared in a volume of 100 ml and at a temperature of 80 °C. Ten millimolars of $Na_2S_2O_3$, 10 mM $CdCl_2$, and 6 and 10 mM H_3BO_3 powder were used in the electrochemical deposition solutions of CdS:B semiconductor thin films. Electrochemical characterization of CdS semiconductor films was investigated by applying the chronoamperometry (CA) technique. IVIUM VERTEX Potentiostat/Galvanostat device, which served as DC supply unit and was set at a constant voltage of 1.8 V for 100 s, was used during the experimental studies. In the system prepared for the experiment, ITO-coated glasses were used for the working electrode, Ag/AgCl for the reference electrode, and platinum wire for the counter electrode. The surface formations of pure and boron-doped CdS thin films were examined by scanning with the ZEISS Supra 40 VP electron microscope (SEM). The percentages of atomic components of these thin films were determined by the energy-dispersive X-ray (EDX) system. X-ray system with CuKα radiation ($\lambda K\alpha$ = 1542 Å) was used to detect the crystal structure of the materials (Panalytical Empyrean). Optical absorption and reflection spectra were measured using UV–vis spectrometer. All of these measurements were carried out at Bilecik Seyh Edebali University Central Research Laboratory. The pictures of the pure and boron-doped CdS semiconductor thin films are given in **Figure 1**.

The thicknesses of the films were calculated using the gravimetric weight difference method with the formula given below[16]:

$$t = \frac{M_s - M_i}{A.\rho} \tag{1}$$

In this method, first, the ITO substrates were weighed one by one on a precision balance before deposition (M_i), and then reweighed (M_s) after the film was formed. M_s–M_i gave the weight of the composed film. Here, ρ is the density of the film and A is the surface area of the ITO substrate. When calculating the film thickness, the film was assumed to be of homogeneous thickness and the density value for CdS and boron was taken as 4.82 and 2.30 g cm^{-3}, respectively.[17]

Additionally, to support the thickness results, Faraday's law has been applied to the electrodeposited film by below formula [18]:

$$T = \frac{(JtM)}{(nF\rho)} \tag{2}$$

Here T is the thickness, J is the current density (A cm^{-2}), t is the deposition time (s), M is the molecular mass (g mol^{-1}), n is the number of electrons required for the deposition, F is the Faraday constant (96 485 C mol^{-1}) and ρ is the density (g cm^{-3}).

The thickness values were found to be 222, 224, and 225 nm for pure, 0.06B, and 0.1B doped CdS films, respectively.

3. Results and Discussion

3.1. XRD Investigations

X-ray diffraction (XRD) is a characterization method used to determine the crystal structure of a material. By analyzing the results obtained as a result of XRD measurements, information about the crystal structure of the material can be obtained. This technique allows the identification, indexing, and quantification of the crystal structure of crystalline phases present in materials. It also provides access to information such as grain size, orientation, and the deformation of the crystal network.[19]

The XRD graphs of pure and boron-doped CdS thin films are given in **Figure 2**a. XRD results are in agreement with reference JPDC 98-015-4186. It is seen that all samples grow in hexagonal structure and crystal orientations are in (100), (002), (101), (110), and (112) directions. The peak intensities decreased with the increase of boron dopant ratio. This behavior indicates that boron doping affects the crystallinity of the thin film. Occupying the intermediate regions of the doping atoms causes deterioration in the crystal structure.[20] As the doping ratio increases, the intensity of the (101) peaks in the diffraction pattern decreases significantly, (100) and (002) peaks seem to disappear completely with the addition of 10 mM boric acid. The decrease in peak intensity indicates that the crystal structure deteriorates with the increase in boron concentration. This may be due to internal stress caused by the smaller ionic radius of boron compared to cadmium and sulfur. Additionally, boron diffraction peaks were observed in the XRD patterns of boron-doped thin films. The reason for this can be said that boron does not penetrate into the inner pores of CdS, but shows itself actively on the surface due to its high Lewis acid feature.[21] In Figure 2b, boron addition shifted the XRD pattern peak to lower positions. This shift was associated with the incorporation (substitution and/or interstitial site) of the doping atom in the crystal lattice of the CdS thin films, and the lower shifts observed in the peak position were due to the effective ionic radius of the doped atoms.[22]

© 2024 Wiley-VCH GmbH

15214079, 2024, 6, Downloaded from https://onlinelibrary.wiley.com/doi/10.1002/crat.202300353 by Bilecik Seyh Edebali, Wiley Online Library on [05/12/2025]. See the Terms and Conditions (https://onlinelibrary.wiley.com/terms-and-conditions) on Wiley Online Library for rules of use; OA articles are governed by the applicable Creative Commons License

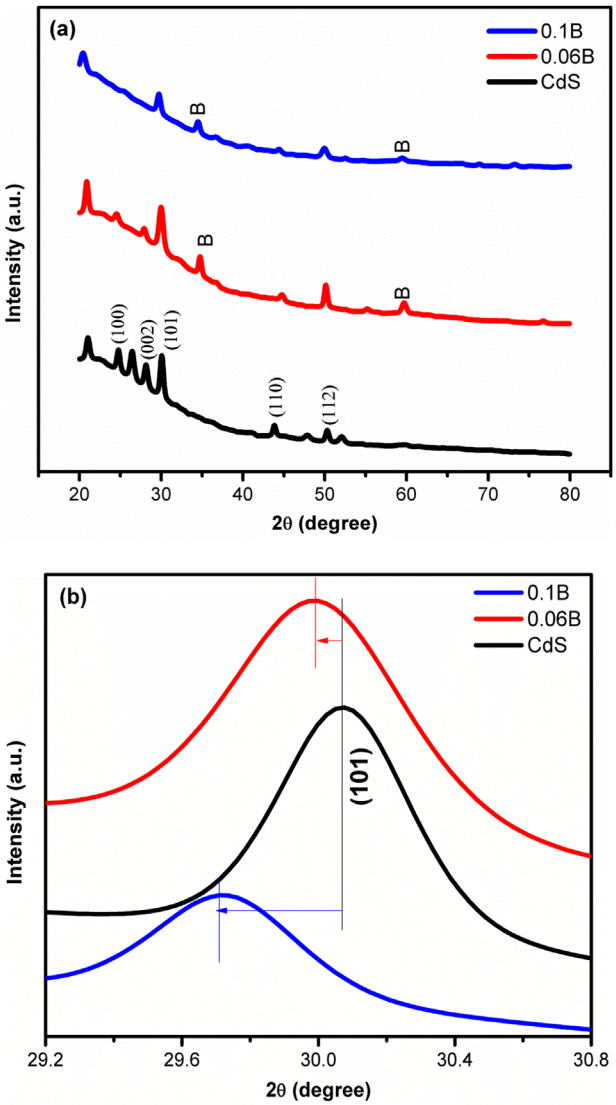

Figure 2. a) XRD patterns and b) peak shifting of pure and boron-doped CdS thin film samples.

The grain sizes of samples are computed with the modified Scherrer plot based on the following formula[23]:

$$\ln \beta = ln\frac{0.9\ \lambda}{D} + ln\frac{1}{\cos\theta} \quad (3)$$

where, "D" is the size of the crystal, "λ" is the wavelength (1.542 Å) of the incident X-ray, β is the full-width half maximum value and the θ is the angle of the pattern from X-ray measurement. If the results for ln β are plotted relative to ln (1/cos θ), a line with an approximate slope and an intersection of ln 0.9λ/D can be obtained. From here, a nano-size D value can be determined. With respect to the computed crystal size values of the samples determined from the intersection point of the graph given in **Figure 3** and **Table 1**, with increasing boron addition, there is a decrease in crystal size. If CdS thin films are doped

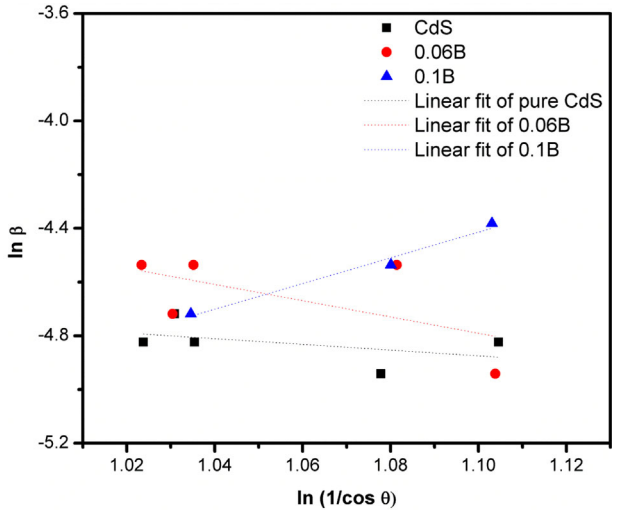

Figure 3. Modified Scherrer equation graph of pure and boron-doped CdS thin film samples.

with atoms of a smaller atomic radius than Cd, the crystal size decreases. The decrease in grain size indicates that the grain boundaries will increase in size and the crystallization of high boron-doped films will deteriorate.[24]

From the above results, it was concluded that boron doping plays an important role in the crystal properties of CdS films and can effectively change the microstructure of CdS films.

3.2. SEM Investigations

SEM images of pure and boron-doped CdS thin films are given in **Figure 4**. SEM images show that the substrate surface is well

Table 1. Getting some structural features of deposited samples (d_{hkl}: interplanar distance, FWHM: full-width half maximum, $D_{SR\text{-}ort}$: crystal size from modified Scherer plot).

	(hkl)	dhkl [Å]	2θ [°]	FWHM[°]	DSR-ort [nm]
pure CdS	(100)	3.5976	24.75	0.4605	17.58
	(002)	3.1736	28.12	0.5117	
	(101)	2.9740	30.05	0.4605	
	(110)	2.0666	43.81	0.4093	
	(112)	1.8151	50.27	0.4605	
0.06 B	(100)	3.6293	24.53	0.6140	14.96
	(002)	3.1970	27.91	0.5117	
	(101)	2.9828	29.96	0.6140	
	(110)	2.0253	44.75	0.6140	
	(112)	1.8209	50.10	0.4093	
0.01 B	(100)	–	–	–	13.41
	(002)	–	–	–	
	(101)	3.0083	29.70	0.5117	
	(110)	2.0401	44.41	0.6140	
	(112)	1.8267	49.93	0.7164	

© 2024 Wiley-VCH GmbH

15214079, 2024, 6, Downloaded from https://onlinelibrary.wiley.com/doi/10.1002/crat.202300353 by Bilecik Seyh Edebali, Wiley Online Library on [05/12/2025]. See the Terms and Conditions (https://onlinelibrary.wiley.com/terms-and-conditions) on Wiley Online Library for rules of use; OA articles are governed by the applicable Creative Commons License

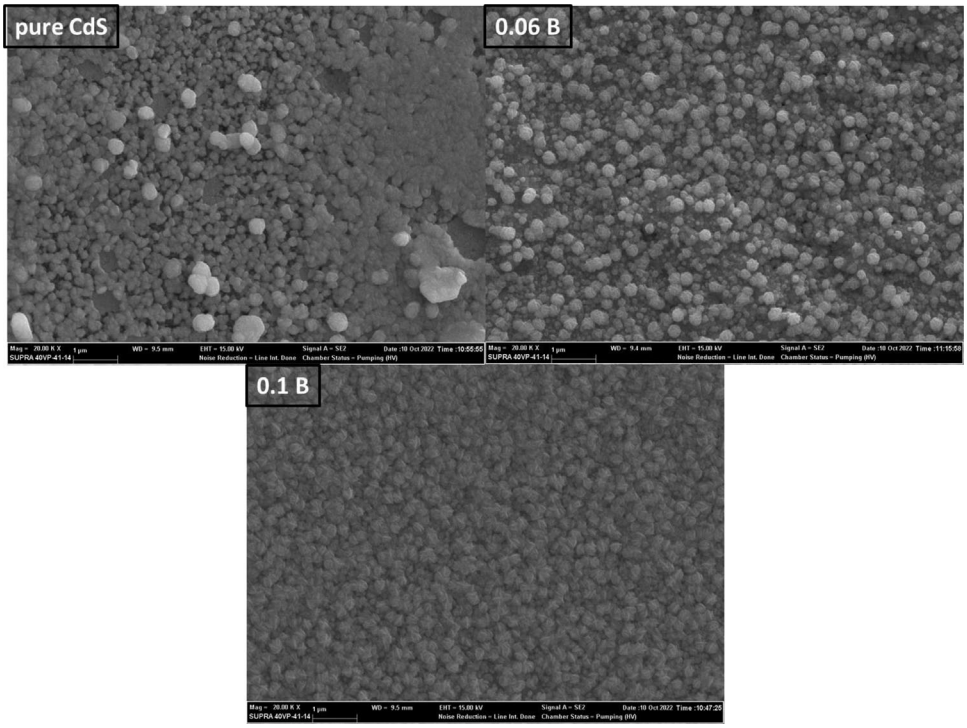

Figure 4. SEM images of pure and boron-doped CdS thin film samples.

coated with the nanostructure. Pure CdS SEM images show that the material is coated on the layer as spheres and is homogeneously distributed. Erturk et al. investigated surface properties of CdS:Zn thin film samples by electrodeposition and they reported enlarged, dense, and uniform thin films, which can be associated with the nano-sized characteristics.[25] The change in the morphology of CdS clusters is visible as the amount of boron dopant amount increases. In general, the formation of self-evolving nanostructure depends on parameters such as thermodynamic environment and crystal growth. Since the radius of the boron is different from that of the cadmium ion, the crystallization properties of CdS changed depending on the amount of boron dopant. Similar morphology with flower-like structures has been reported for tartaric acid-doped CdS films.[26] The size of the particles decreased with increasing boron contribution.

EDX is a common method used to perform elemental analysis of a sample. X-rays are emitted when the high-energy electron beams of the SEM device interact with the sample. These X-rays carry the energies of the elements that make up the material. Thus, they provide data on the chemical composition of the sample.[27]

The EDX measurement results of the percentages of elements in the structure of the pure and boron-doped CdS semiconductor thin film are shown in **Figure 5**. The peaks in the spectrum correspond to the characteristic emission energies of the elements in the structure. The percentages of Cd, B, and S elements in the structure can be seen from the EDX analysis results. The result is in agreement with similar compositional analysis for selenous acid-doped CdS thin films.[28]

3.3. Optical Investigations

3.3.1. Absorbance, Transmittance, and Optical Bandgap

When a photon (light beam) of different frequencies arrives on any semiconductor, an interaction occurs between the electrons of the atoms and the incident photon, and depending on the type of this interaction, the optical properties of materials such as absorption, transmittance, and reflection emerge.[29] The absorbance of a material is determined by the intensity of radiation absorbed by a material, by the amount of incident radiation intensity. In order to examine thin film; reflection, absorption, and transmission are the most important properties that help to know the behavior of materials and media when attracted by light.[30]

The absorbance spectra of pure and boron-doped CdS semiconductor thin films are given in **Figure 6**. It is seen that all electrodeposited films have low absorption in the wavelength range of 550–1000 nm and the sharp increase in absorbance values for all films is realized at wavelengths less than 550 nm. By comparing the absorbance diagrams of pure and boron-doped CdS, the sharpness of the peak at low wavelengths is reduced by adding boron. This decrease in the sharpness of the peak continues with an increase in the amount of boron due to the decrease in crystallinity. Similar absorbance behavior was observed in neodymium additives in cadmium sulfide thin films.[31]

According to the transmittance spectra of pure and boron-doped CdS semiconductor thin films shown in **Figure 7**, the films in the visible area have a very transparent structure. An average transmittance of 55%, 78%, and 81% was determined for pure

© 2024 Wiley-VCH GmbH

15214079, 2024, 6, Downloaded from https://onlinelibrary.wiley.com/doi/10.1002/crat.202300353 by Bilecik Seyh Edebali, Wiley Online Library on [05/12/2025]. See the Terms and Conditions (https://onlinelibrary.wiley.com/terms-and-conditions) on Wiley Online Library for rules of use; OA articles are governed by the applicable Creative Commons License

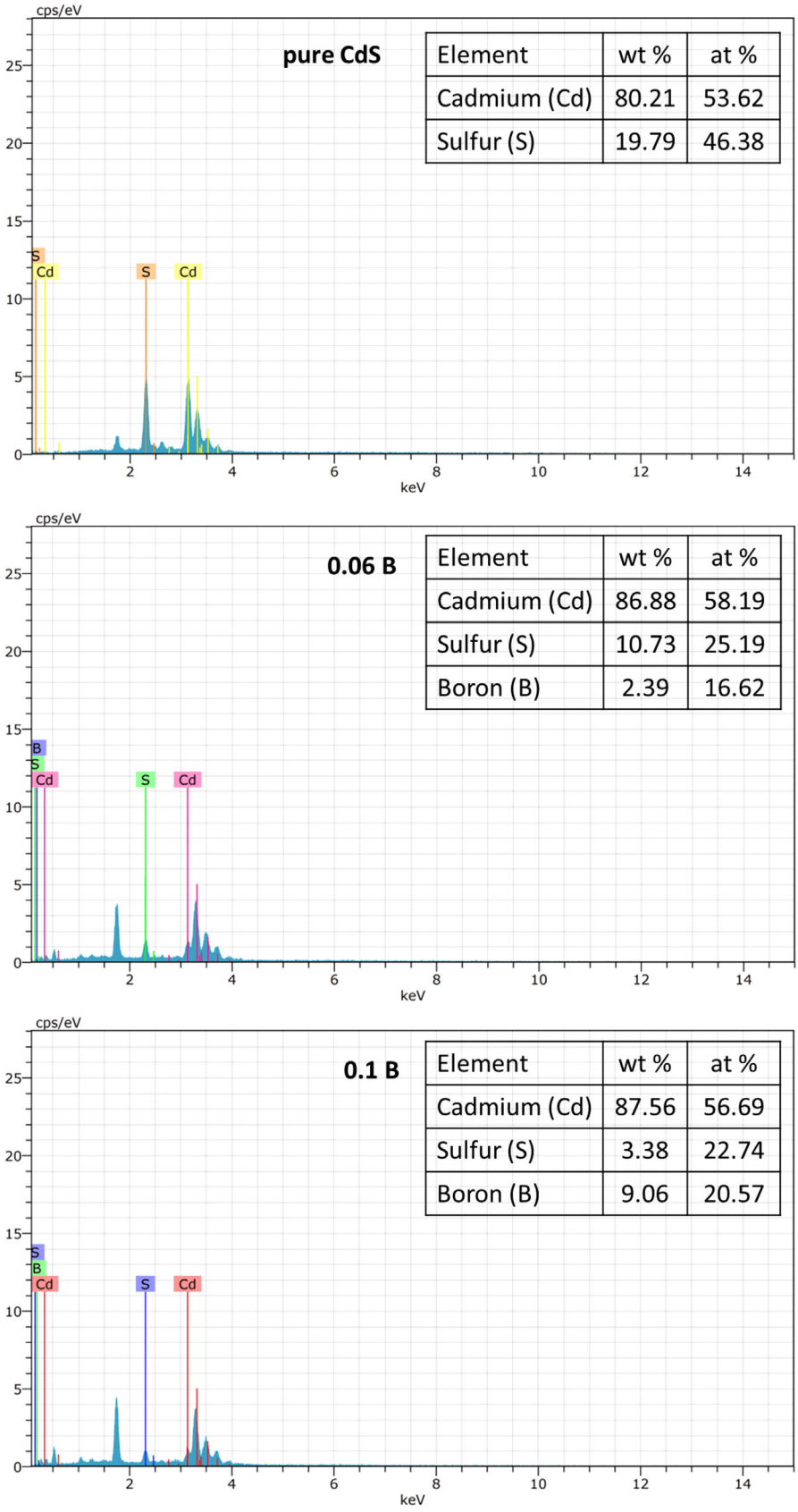

Figure 5. EDX graph and compositions of pure and boron-doped CdS samples.

© 2024 Wiley-VCH GmbH

15214079, 2024, 6, Downloaded from https://onlinelibrary.wiley.com/doi/10.1002/crat.202300353 by Bilecik Seyh Edebali, Wiley Online Library on [05/12/2025]. See the Terms and Conditions (https://onlinelibrary.wiley.com/terms-and-conditions) on Wiley Online Library for rules of use; OA articles are governed by the applicable Creative Commons License

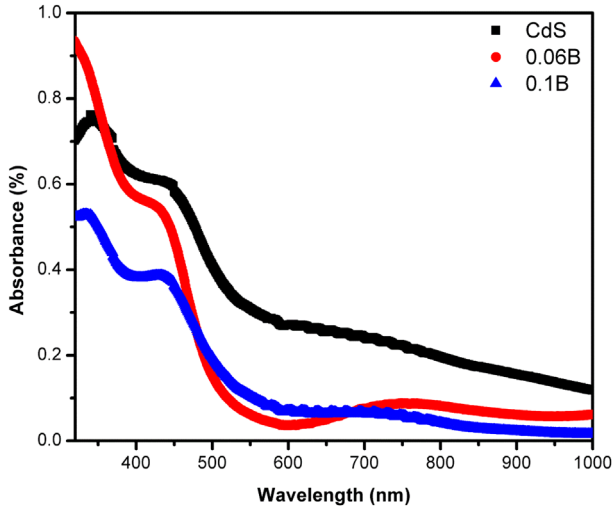

Figure 6. Optical absorption spectra of the CdS films with boron dopant.

CdS films, 0.06 B and 0.1B doped CdS films, respectively in the range of 550–1000 nm. The doping rate had a significant effect on the optical transmittance of the films. This result can be attributed to the reduction of the voids in the film and the healing of the homogeneous structure with uniformly distributed particles, thereby increasing the optical scattering. In addition, as can be seen from the SEM images, the decrease in surface roughness and the resulting increase in transparency as a result of the uniform condensation of the grains between each other may also play a role in increasing the optical transmittance. C. Liu et al. investigated the transmittance of the Ta-doped InTe thin films and they reported that the transmittance is nearly 84% in the transparence region and the value of transmittance increases after Ta doping.[32]

The optical bandgap of the pure CdS semiconductor thin films was calculated as 2.14 eV. Optical bandgap values of 0.06 and 0.1 M boron-doped CdS semiconductor thin films were found

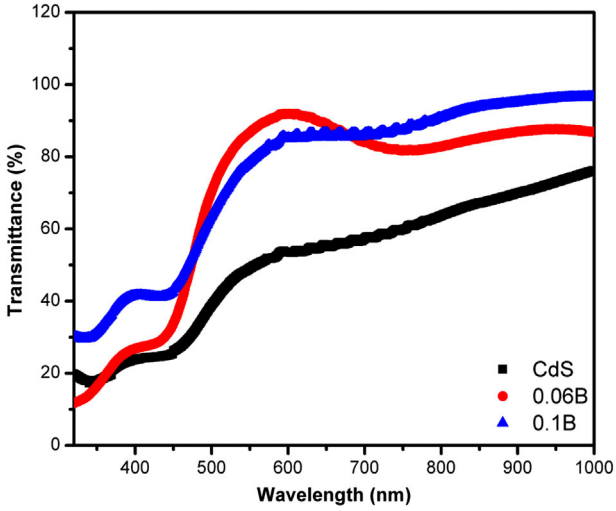

Figure 7. Optical transmittance spectra of the CdS films with boron dopant.

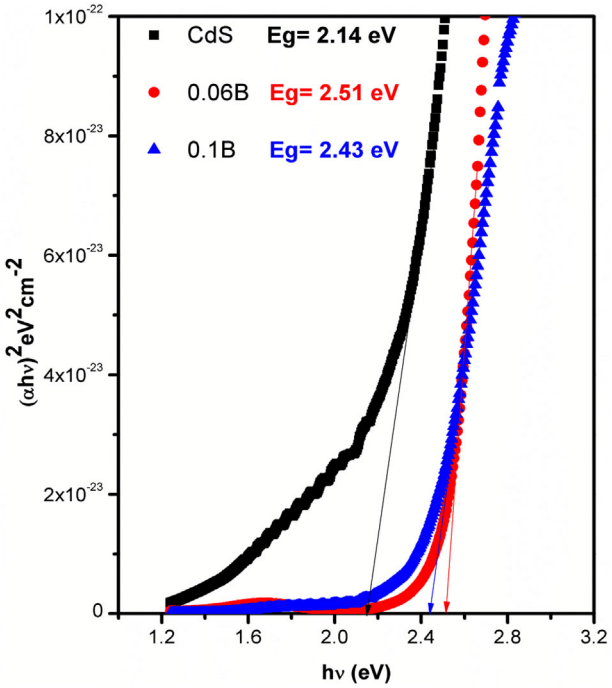

Figure 8. $(\alpha h\upsilon)^2$-$h\upsilon$ spectrum of CdS films with boron dopant.

to be 2.51, and 2.43 eV respectively. (See **Figure 8**). As the boric acid concentration increases up to 0.06 M, the value of the optical bandgap energy increases, resulting in the deterioration of crystallization. Another reason for the decrease in the optical bandgap energy of the films after a 0.06 M boron doped CdS with the increasing amount of dopant can be interpreted as the result of the intermediate energy states formed by the impurities in the structure formed at high speed.[33] Yücel and Kahraman reported a reduction in optical bandgap values of both the coated and annealed coumarin-doped CdS films by chemical route with rising doping concentration.[34]

3.3.2. Optical Constants (n,k) and Skin Depth

The refractive index of a substance is the coefficient showing how slow the light or other electromagnetic waves traveling through that substance move compared to the light traveling ina vacuum. The graphs of the change of refractive indexes of pure and boron-doped CdS thin films with wavelength are given in **Figure 9**. The refractive index was obtained using the below equation[35]:

$$n = \frac{1+R}{1-R} + \sqrt{\frac{4R}{(1-R)^2} - k^2} \tag{4}$$

where R is the reflection coefficient and k is the extinction coefficient.

When Figure 9 is examined carefully, the refractive indexes of the pure, 0.06, and 0.1 M boron-doped CdS thin films in the whole spectrum (400–1000 nm) are 2.37, 1.75, and 1.63, respectively. The refractive index n decreases exponentially as the wavelength increases. It was seen that the refractive index values of the boron

© 2024 Wiley-VCH GmbH

15214079, 2024, 6, Downloaded from https://onlinelibrary.wiley.com/doi/10.1002/crat.202300353 by Bilecik Seyh Edebali, Wiley Online Library on [05/12/2025]. See the Terms and Conditions (https://onlinelibrary.wiley.com/terms-and-conditions) on Wiley Online Library for rules of use; OA articles are governed by the applicable Creative Commons License

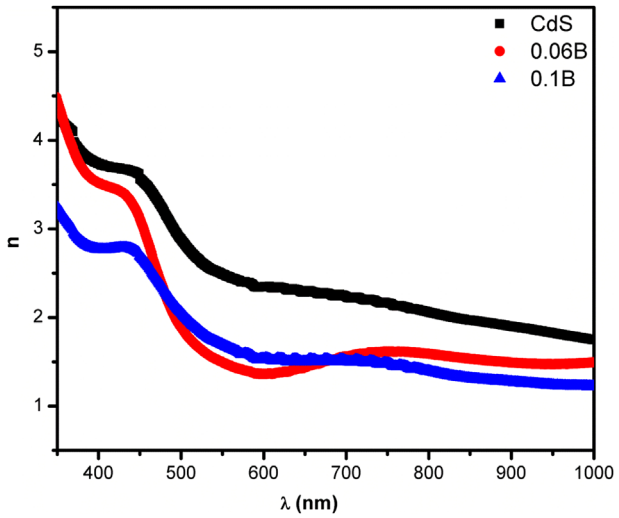

Figure 9. The variation of refractive index with wavelength for pure and boron-doped CdS.

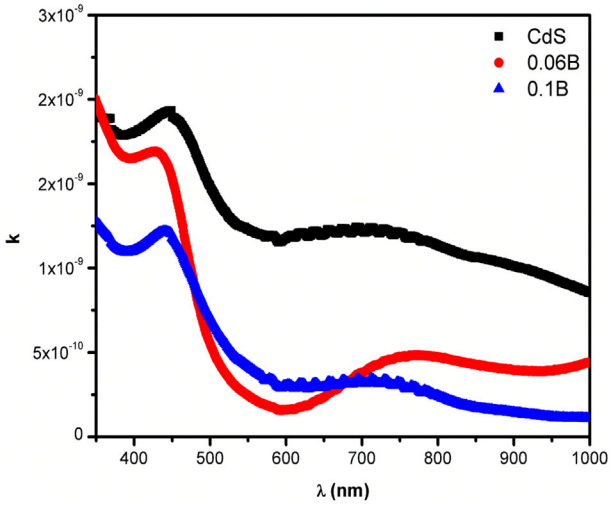

Figure 10. The graphical representation between the extinction coefficient of pure and boron-doped CdS thin films and photon wavelength.

dopant reduced in comparison with the pure CdS thin film. The decline in the value of the refractive index is because of the optical dispersion behavior of the material.[36] Also, the refractive index of boron-doped CdS films is less than that of the pure CdS film. A similar observation was reported for PbS/PVA nano polymer composite.[37] The reason for this may be that the presence of boron elements in the CdS structure reduces the polarization ability of the electrons.

One of the important parameters used to describe the optical properties that determine how light interacts with a material is the extinction coefficient. The extinction coefficients were calculated using the equation below[38]:

$$k = \frac{\alpha\lambda}{4\pi} \tag{5}$$

where α is the absorption coefficient and λ is the wavelength. The graphs of variation of extinction coefficients of pure and boron-doped CdS thin films with wavelength are given in **Figure 10**. It can be seen from Figure 10; that as the wavelength increases, the extinction coefficient k decreases exponentially. The value of k for pure and doped-CdS agrees well with the literature refs. [39, 40] The extinction coefficients were observed to vary in the range of 1.25×10^{-9}–5.26×10^{-10} values. It is therefore observed that there is a partial decrease in the extinction coefficient with an increase in the amount of boron dopant. The low value of the extinction coefficient in the spectrum demonstrates the surface smoothness and high transmittance of the films. This is fully consistent with the images obtained from SEM and the transmittance spectrum.

The amplitude of the electromagnetic wave decreases after penetrating a certain unit thickness; this is called the skin depth (δ). More simply, the surface depth value provides an estimate of the distance at which light passes through a semiconductor. The skin depth of thin films of different thicknesses was evaluated by the following relation:[41]

$$\delta = \frac{1}{\alpha} = \frac{\lambda}{2\pi k} \tag{6}$$

where λ is the wavelength of the photon and k is the extinction coefficient. Skin depth versus photon energy of thin films is shown in **Figure 11**. It was found that δ values of thin films decreased with increasing photon energy. The same behavior was observed as the skin depth increased with increasing NiO content in NiO:Fe_2O_3 thin films prepared by spray technique.[42] This is due to the inverse correlation between the skin depth and the absorption coefficient.

3.3.3. Dielectric Properties

The polarizability of a solid is related to the density of states within the forbidden bandgap. The complex dielectric function (ε^*) of the solid is as follows[43]:

$$\varepsilon^* = \varepsilon_1 + i\varepsilon_2 = (n + ik)^2 \tag{7}$$

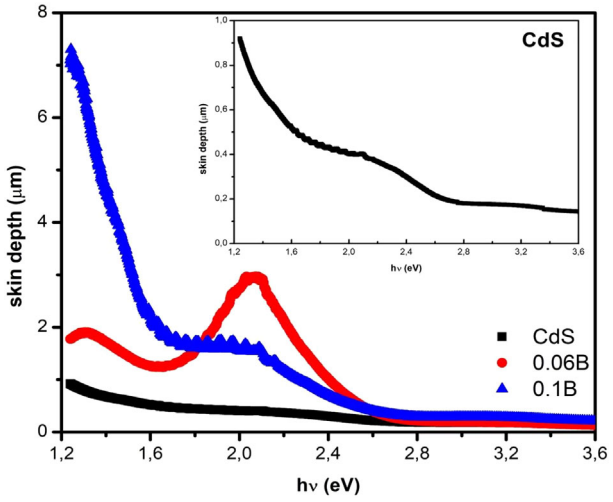

Figure 11. Pure and boron-doped CdS skin depth graph on ITO substrate.

© 2024 Wiley-VCH GmbH

15214079, 2024, 6, Downloaded from https://onlinelibrary.wiley.com/doi/10.1002/crat.202300353 by Bilecik Seyh Edebali, Wiley Online Library on [05/12/2025]. See the Terms and Conditions (https://onlinelibrary.wiley.com/terms-and-conditions) on Wiley Online Library for rules of use; OA articles are governed by the applicable Creative Commons License

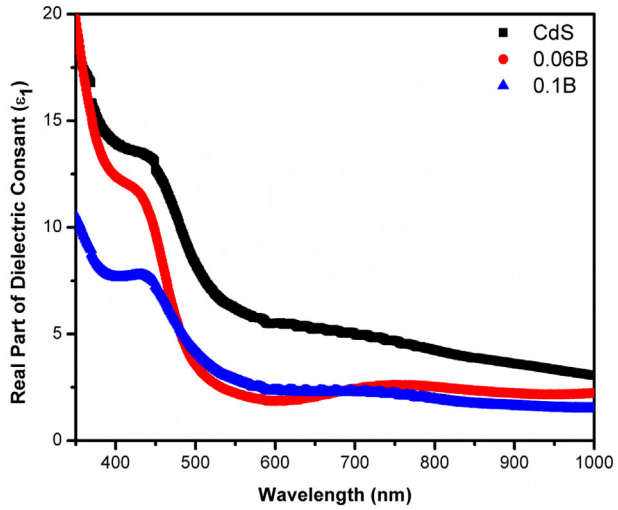

Figure 12. The real part of the dielectric constant for pure and boron-doped CdS.

here ε_1 is the real part of the dielectric constant, that is, the energy stored in the solid and ε_2 is the imaginary part of the dielectric constant associated with the dispersion energy in the solid. From Equation (6), it can be obtained the following relations:[44]

$$\varepsilon_1 = n^2 - k^2 \tag{8}$$

$$\varepsilon_2 = 2nk \tag{9}$$

The ε_1 and ε_2 values for thin films were calculated using the above equations and plotted as a function of λ. ε_1 and ε_2 values change with λ for all films in the same way. **Figures** 12 and 13 show the variation of the imaginary and real parts of the dielectric constant of the pure and boron-doped CdS films against the wavelength, respectively. As can be seen from the figures, the real part of the dielectric constant was found to be higher than the imaginary part. Similar results were observed for Cu-doped CdS

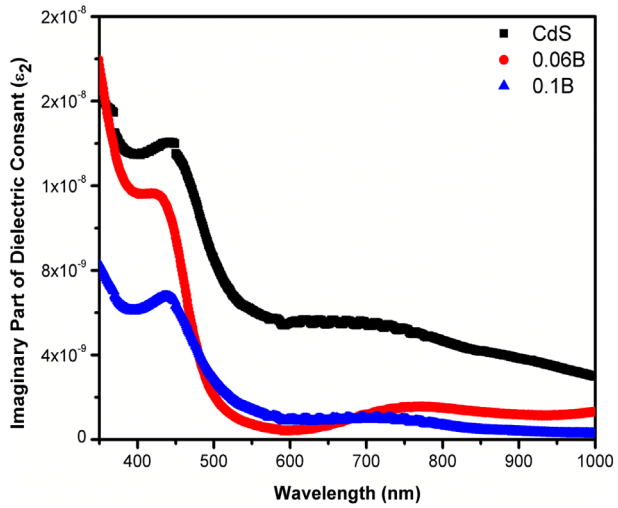

Figure 13. The imaginary part of the dielectric constant for pure and boron-doped CdS.

reported by reference of.[45] The dielectric parameters depend on the refractive index values increase due to improved film crystallization and reduction of interatomic plane distances, as well as lessening voids and crystal defects. A similar observation was reported for sprayed Gd-doped CdS thin films.[46] It was evaluated that the dielectric constants of the films could be changed with the boron dopant. M. Shkir et al. investigated imaginary and real parts of dielectric constants for pure and Pr-doped CdS films over a broad wavelength range. They reported that these constants showed oscillatory behavior in the higher wavelength region.[47]

4. Conclusion

In this study, boron-doped and pure CdS semiconductor thin films prepared by the electrodeposition method were synthesized and the structural and optical properties of these films were investigated. In light of the analysis carried out, it was observed that the structural and optical properties of the films were strongly dependent on the boron concentration. According to X-ray reflection peaks in different planes, the films were polycrystalline over the entire examined boron additive concentration range. The density of the peaks and their crystal orientation depend on the boron dopant concentration. There is a decrease in the grain size of the films in addition to boric acid concentration. According to the absorption spectra of pure and boron-doped CdS films, it is seen that the films have low absorption in the 550–700 nm wavelength range. The films in the visible area have a very transparent structure. Micrographs show a uniform film structure with distinct grain boundaries. The boron atoms can affect the grain size. The surface morphology of the films is largely dependent on the boric acid concentration. EDX pattern for films contains cadmium, sulfur, and boron. With these spectra, it has been seen that there are expected elements in solid films. By using the absorption spectrum of CdS:B semiconductor films, the optical bandgap energies of the films were determined. Since the particle size of the films decreased with the excess of boron doping, the optical bandgap of these films increased. It has been determined that the optical bandgap of the excessively boron-doped CdS films is wider than that of the pure CdS films. These results emphasize the importance of the effect of dopant concentration on optical behavior. The wide bandgap is important for the window layer in solar cell applications. Consequently, the use of boron-doped CdS semiconductor thin film will be important in solar cell applications.

Acknowledgements

The author had not received funding (institutional, private, and/or corporate financial support) for the work reported in the manuscript.

Conflict of Interest

The authors declare no conflict of interest.

Author Contributions

E.E. contributed to the design and implementation of the research, to the analysis of the results, and to the writing of the manuscript.

© 2024 Wiley-VCH GmbH

15214079, 2024, 6, Downloaded from https://onlinelibrary.wiley.com/doi/10.1002/crat.202300353 by Bilecik Seyh Edebali, Wiley Online Library on [05/12/2025]. See the Terms and Conditions (https://onlinelibrary.wiley.com/terms-and-conditions) on Wiley Online Library for rules of use; OA articles are governed by the applicable Creative Commons License

Data Availability Statement

The data that support the findings of this study are available on request from the corresponding author. The data are not publicly available due to privacy or ethical restrictions.

Keywords

boron-doped Cds, electrodeposition, optical properties, semiconductor films, structural properties

Received: December 27, 2023
Revised: March 6, 2024
Published online: April 9, 2024

[1] S. M. Sze, Y. Li, K. K. Ng, *Physics of Semiconductor Devices*, 4th ed, John Wiley & Sons, Hoboken, New Jersey **2021**, 944.
[2] O. K. Echendu, S. Z. Werta, F. B. Dejene, K. O. Egbo, *J. Alloys. Compd.* **2019**, *778*, 197.
[3] H. Dabhane, S. Ghotekar, P. Tambade, S. Pansambal, H. A. Murthy, R. Oza, V. Medhane, *Environ. Chem. Ecotoxicol* **2021**, *3*, 209.
[4] D. Berman-Mendoza, O. I. Diaz-Grijalva, R. López-Delgado, A. Ramos-Carrazco, M. E. Alvarez-Ramos, F. Romo-Garcìa, H. J. Higuera-Valenzuela, R. Rangel, *J. Mater. Sci: Mater. Electron.* **2021**, *32*, 25462.
[5] A. Kathalingam, S. Valanarasu, T. Ahamad, S. M. Alshehri, H. S. Kim, *Ceram. Int* **2021**, *47*, 7608.
[6] R. Bairy, A. Jayarama, G. K. Shivakumar, S. D. Kulkarni, S. R. Maidur, P. S. Patil, *Physica B Condens. Matter* **2019**, *555*, 145.
[7] V. S. Meena, A. K. Saini, D. K. Rana, M. S. Mehata, *Mater. Today: Proc* **2022**, *67*, 643.
[8] C. Doroody, K. S. Rahman, H. N. Rosly, M. N. Harif, M. Isah, Y. B. Kar, S. K. Tiong, N. Amin, *Mater. Sci. Semicond. Process.* **2021**, *133*, 105935.
[9] N. J. Ghdeeb, *Int. J. Thin Film Sci. Tec.* **2022**, *11*, 115.
[10] K. H. Chol, C. H. Ho, K. Y. Jo, S. G. Il, *Opt. Mater.* **2021**, *112*, 110790.
[11] A. S. Gadalla, H. A. Al-Shamiri, S. M. Alshahrani, H. F. Khalil, M. M. El Nahas, M. A. Khedr, *Coatings* **2022**, *12*, 87.
[12] A. E. Alam, W. M. Cranton, I. M. Dharmadasa, *J. Mater Sci: Mater Electron.* **2019**, *30*, 4580.
[13] H. I. Salim, O. I. Olusola, A. A. Ojo, K. A. Urasov, M. B. Dergacheva, I. M. Dharmadasa, *J. Mater Sci: Mater Electron.* **2016**, *27*, 6786.
[14] U. Saraç, M. Kaya, M. C. Baykul, *Dig. J. Nanomater. Biostructures* **2021**, *16*, 1137.
[15] A. I. Kaya, *J. Thermoplast. Compos. Mater.* **2022**, *35*.
[16] N. Nobari, M. Behboudnia, R. Maleki, *Mater. Sci. Eng. B* **2017**, *224*, 181.
[17] B. Altiokka, A. K. Yildirim, *J. Korean Phys. Soc.* **2018**, *72*, 687.
[18] A. A. Ojo, I. M. Dharmadasa, *J. Mater Sci: Mater Electron.* **2017**, *28*, 14110.
[19] E. Erdoğan, M. Kundakçı, *Microelectron. Eng.* **2019**, *207*, 15.
[20] S. Z. Werta, O. K. Echendu, F. B. Dejene, *J. Mater Sci: Mater Electron.* **2019**, *30*, 6201.
[21] V. Nori, F. Pesciaioli, A. Sinibaldi, G. Giorgianni, A. Carlone, *Catalysts* **2021**, *12*, 5.
[22] O. K. Echendu, S. Z. Werta, F. B. Dejene, A. A. Ojo, I. M. Dharmadasa, *J. Mater Sci: Mater Electron.* **2019**, *30*, 4977.
[23] E. Erdoğan, *Indian J. Phys.* **2019**, *93*, 1313.
[24] B. Lohitha, S. Thanikaikarasan, S. R. Marjorie, *Mater. Today: Proc* **2020**, *33*, 3068.
[25] K. Erturk, M. Isik, M. Terlemezoglu, N. M. Gasanly, *Opt. Mater.* **2021**, *114*, 110966.
[26] D. Boosagulla, S. Mandati, R. Allikayala, B. V. Sarada, *Thin Solid Films* **2022**, *741*, 139011.
[27] A. M. Elbarbary, M. Bekhit, F. I. A. El Fadl, R. Sokary, *J. Inorg. Organomet. Polym. Mater.* **2022**, *32*, 383.
[28] J. Maricheva, S. Bereznev, N. Maticiuc, O. Volobujeva, J. Kois, *Electrochim. Acta* **2017**, *242*, 280.
[29] A. S. Hassanien, A. A. Akl, *Appl. Phys. A* **2018**, *124*, 752.
[30] E. Erdogan, *Surf. Rev. Lett.* **2021**, *28*, 2150081.
[31] K. V. Chandekar, M. Shkir, T. Alshahrani, A. Khan, S. AlFaify, *Chin. J. Phys.* **2020**, *67*, 681.
[32] C. Liu, Y. Yuan, X. Zhang, J. Su, X. Song, H. Ling, Y. Liao, H. Zhang, Y. Zheng, J. Li, *Nanomaterials* **2020**, *10*, 1887.
[33] A. J. Jebathew, M. Karunakaran, R. Ade, N. D. Jayram, V. Ganesh, Y. Bitla, S. Vinoth, H. Algarni, I. S. Yahia, *Opt. Mater.* **2021**, *117*, 111177.
[34] E. Yücel, S. Kahraman, *Ceram. Int.* **2015**, *41*, 4726.
[35] E. Erdoğan, G. Turgut, M. Yilmaz, *Optik* **2021**, *240*, 166819.
[36] D. Herrera-Molina, J. E. Diosa, A. Fernández-Pérez, E. Mosquera-Vargas, *Mater. Sci. Eng. B* **2021**, *273*, 115451.
[37] M. S. Ismail, A. A. Elamin, F. Abdel-Wahab, Y. H. Elbashar, M. M. Mahasen, *Opt. Mater.* **2022**, *131*, 112639.
[38] Z. K. Heiba, M. B. Mohamed, S. I. Ahmed, *Appl. Phys. A* **2021**, *127*, 577.
[39] Z. R. Khan, M. Shkir, V. Ganesh, S. AlFaify, I. S. Yahia, H. Y. Zahran, *J. Electron. Mater.* **2018**, *47*, 5386.
[40] M. Shkir, I. M. Ashraf, K. V. Chandekar, I. S. Yahia, A. Khan, H. Algarni, S. AlFaify, *Sens. Actuator A Phys.* **2020**, *301*, 111749.
[41] A. R. Wassel, I. M. El Radaf, *Appl. Phys. A* **2020**, *126*, 177.
[42] S. S. Chiad, *Int. Lett. Chem. Phys. Astron.* **2015**, *6*, 50.
[43] H. Chenaina, C. Messaadi, J. Jalali, H. Ezzaouia, *Inorg. Chem. Commun.* **2021**, *124*, 108401.
[44] E. Erdoğan, A. Kiyak Yildirim, *J. Mater Sci: Mater Electron.* **2023**, *34*, 880.
[45] M. Shkir, Z. R. Khan, M. Anis, S. S. Shaikh, S. AlFaify, *Chin. J. Phys.* **2020**, *63*, 51.
[46] M. Shkir, K. V. Chandekar, A. Khan, A. M. El-Toni, I. M. Ashraf, M. Benghanem, S. F. Adil, A. A. Ansari, H. Ghaithan, S. AlFaify, *Mater. Chem. Phys.* **2020**, *255*, 123615.
[47] M. Shkir, I. M. Ashraf, S. AlFaify, A. M. El-Toni, M. Ahmed, A. Khan, *Ceram. Int.* **2020**, *46*, 4652.

© 2024 Wiley-VCH GmbH

15214079, 2024, 6, Downloaded from https://onlinelibrary.wiley.com/doi/10.1002/crat.202300353 by Bilecik Seyh Edebali, Wiley Online Library on [05/12/2025]. See the Terms and Conditions (https://onlinelibrary.wiley.com/terms-and-conditions) on Wiley Online Library for rules of use; OA articles are governed by the applicable Creative Commons License